

# Signal detection based on empirical mode decomposition and Teager–Kaiser energy operator and its application to P and S wave arrival time detection in seismic signal analysis

Ismail Kirbas<sup>1</sup> · Musa Peker<sup>2</sup>

Received: 13 April 2016 / Accepted: 21 April 2016 / Published online: 28 April 2016  
© The Natural Computing Applications Forum 2016

**Abstract** Determining P and S wave arrival times while minimizing noise is a major problem in seismic signal analysis. Precise determination of earthquake onset arrival timing, determination of earthquake magnitude, and calculation of other parameters that can be used to make more accurate seismic maps are possible with the detection of these waves. Experts try to determine these waves by manual analysis. But this process is time-consuming and painful. In this study, a new method that enables the determination of P and S wave arrival times in noisy recordings is recommended. This method is based on the hybrid usage of empirical mode decomposition and Teager–Kaiser energy operator algorithms. The results show that the proposed system gives effective results in the automatic detection of P and S wave arrival times. Promisingly, the recommended system might serve as a novel and powerful candidate for the effective detection of P and S wave arrival time.

**Keywords** Empirical mode decomposition · Seismic wave analysis · Teager–Kaiser energy operator · P and S wave detection · Seismic wave arrival time detection

## 1 Introduction

Seismic signals constitute one of the most important subjects in signal analysis. P and S waves, sampling frequency and parameters such as the presence of noise in records are essential for the analysis of seismic signals [1–4]. These analyses provide great benefit in preventing disaster thanks to the rapid determination of the earthquake magnitude and prediction of earthquake occurrence time [5]. There are two main types of seismic waves: surface waves and body waves. Body waves can be classified into two main groups: longitudinal waves (P waves) and transversal waves (S waves). Particle motion and wave propagation speed of different types of waves are also different from each other. Particle movement of P waves is in the direction of wave propagation. In other words, a particle affected by a P wave makes a forward–backward vibration movement in the direction of wave propagation while losing its equilibrium state. The S wave particle motion is on a plane perpendicular to the wave propagation direction. Therefore, the S wave can be separated into horizontal and vertical components [6]. The presence of noise in the records makes the detection of P and S wave arrival times quite difficult. These tasks are usually accomplished by an analyst who chose arrival times based on personal experiences and includes a large amount of pattern recognition. With the increase in the number of digital seismic networks being built in the world, there is an urgent need for a more trustworthy, objective, robust, and less timewasting alternative automated system.

Automatic detection methods for specified purposes are available in the literature. For this problem, Gelchinsky and Shtivelman [7] have used the spatial correlation characteristic of the signal. McCormack et al. [8] developed a method based on feedback neural network algorithm.

---

✉ Ismail Kirbas  
ismailkirbas@mehmetakif.edu.tr

Musa Peker  
musa@mu.edu.tr

<sup>1</sup> Department of Computer Engineering, Faculty of Engineering and Architecture, Mehmet Akif Ersoy University, Burdur, Turkey

<sup>2</sup> Department of Information Systems Engineering, Mugla Sıtkı Kocman University, Muğla, Turkey

Boschetti et al. [9] identified arrival time using fractal dimensions methods. Tong and Kennett [10] used a simple amplitude and energy threshold for determining the P and S wave arrival times. Wagner and Owens [11] used principal eigenvalue as a detector in the frequency area. Withers et al. [12] have methodically compared some trigger algorithms. Aimed at this problem, Hidani and Yamanaka [13] proposed sophisticated pattern recognition, adaptive, and neural network-based approaches. Zhang et al. [14] have used multi-scale wavelet analysis for single-component recordings. Takanami and Kitagawa [15] have used a dual autoregressive model approach and wavelet transformation for the determination of P wave and S wave, respectively. Colak et al. [2] used the wavelet method and the average energy value for the detection of this wave arrival time in three-component stations. Hafez et al. [16] used wavelet filter banks in order to determine P wave arrival time. Liu [17] has used a method called wavelet transform modulus maxima to determine P wave arrival time. Hafez et al. [18] proposed a method based on maximal-overlap discrete wavelet transform to determine P wave arrival time. In addition, other methods such as short- and long-term average rate (STA/LTA) and improved energy ratio [19, 20], wave polarization [21, 22], artificial neural network [23–25], wavelet-based methods [1, 14, 18, 26], spectrogram-based methods [27, 28], autoregressive techniques [29], local-maxima distribution [30], higher order statistics [31, 32], and manifold-based approach [33] have also been proposed for determining the arrival time of these waves. Aboamer et al. [46] proposed a linear model-based estimation method for blood pressure and cardiac output for normal and paranoid cases. Also, Aboamer et al. [47] used the nonlinear features of heart rate variability of paranoid schizophrenic.

In this study, a new method has been developed for the automatic detection of P and S wave arrival times. The developed method is based on hybrid usage of empirical mode decomposition (EMD) and Teager–Kaiser energy operator (TKEO) algorithms. When the literature is examined, it is seen that wavelet and Fourier transform methods have been widely used in seismic signal analysis. The advantage of EMD for time–frequency analysis [e.g., short-term Fourier transform (STFT) or wavelet transform] compared to other existing methods is that EMD is focused entirely on data and it does not impose any predefined assumptions about the signal. Therefore, this method allows the extraction of signal properties in a natural way. EMD is an effective method for adaptive multi-scale analysis of nonlinear and nonstationary signals. What EMD's results will be in wave detection in seismic signals with this interesting feature of EMD was a matter of curiosity. In the second stage of the proposed method, energy changes are examined with a TKEO

algorithm. A noteworthy aspect of the TKEO is that it is almost instantaneous, because only three samples are required each time for energy calculation. It has been found that this nonlinear operator has many impressive features such as simplicity, productivity, and ability to monitor instantly changing spatial patterns. In this study, P and S wave arrival times in the seismic signals are detected efficiently with the application of these two powerful methods.

## 2 Materials and methods

### 2.1 Data

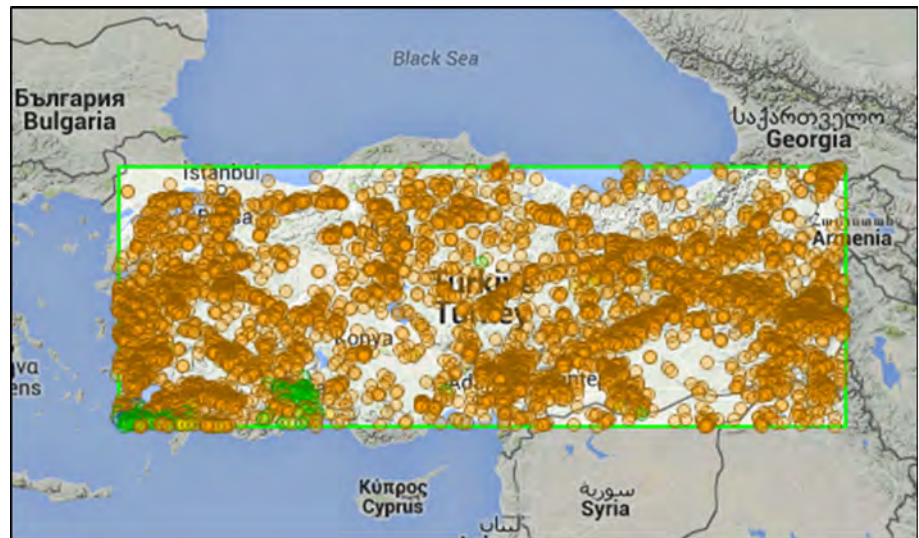
The data used in this study have been taken from the Incorporated Research Institutions for Seismology (IRIS) database [34]. IRIS is a consortium of more than 120 US universities devoted to the operation of science facilities for the organization, acquisition, and distribution of seismological data. The received data are composed of the earthquake data between the years of 2000 and 2015 in Turkey. In order to make certain that they sustain different seismic noise conditions, these earthquakes have different magnitudes (between 3 and 8) and occurred at different times. Figure 1 shows the area where the earthquakes have occurred. 2000 segments were used from more than 10,000 earthquake data. The segments are short-period and very broadband records. Each segment that consists of 2 min has P and S waves.

### 2.2 Empirical mode decomposition

EMD is a nonlinear and adaptive signal decomposition method. EMD, unlike the Fourier transform, makes no assumption of linearity or stability, and unlike the wavelet transforms, it does not include base functions and fixed frequency scale connected to these functions [35]. Compared to Fourier and wavelet transforms, thanks to these features EMD offers a more successful decomposition especially for nonlinear and nonstationary data [3]. As a result of EMD, a finite number of intrinsic mode functions (IMF) and a residue are obtained from the data. IMFs include local instantaneous frequencies, low level IMFs include high local frequencies, and high level IMFs include low local frequencies [3]. All the IMFs must fulfill two conditions:

1. Zero crossing and local extreme numbers of each IMF must be equal or the difference should be 1.
2. Means of upper and lower envelopes obtained from maximum and minimum points must be equal to zero at each point.

**Fig. 1** Map of Turkey region presenting the location and local magnitude of the events logged by different stations



The recursive approach used to obtain the IMFs is as follows [36]:

1. All local extreme points of the signal are extracted.
2. Upper envelope  $e_{\max}(m, n)$  and lower envelope  $e_{\min}(m, n)$  are obtained by interpolating maximum and minimum points.
3. The mean envelope is obtained by the mean of the upper and lower envelopes.

$$\text{mean}(m, n) = (e_{\max}(m, n) + e_{\min}(m, n))/2 \quad (1)$$

4. The mean envelope signal is extracted from the input signal.

$$h(m, n) = \text{input}(m, n) - \text{mean}(m, n) \quad (2)$$

5. It is checked whether the mean envelope signal is close enough to zero or not (the stopping criteria of the IMF).

$$\frac{\sum_{m=1}^W \sum_{n=1}^H |e_{\text{ort}}(m, n)|}{W \times H} < \tau \quad (3)$$

In this equation,  $W$  and  $H$  are spatial dimensions;  $\tau$  is the empirically determined threshold value which is close to zero.

6. If the stop criterion is not met, the  $h(m, n)$  signal (from Step 1) is selected as the new input signal and the process is repeated. If the stop criterion is met,  $h(m, n)$  is taken as new  $\text{IMF}_i$ .

$$\text{IMF}_i(m, n) = h(m, n) \quad (4)$$

7. In order to extract the next IMF, the residual signal from the Step 1 is taken as the new input signal and it is resumed. This process is continued until there is not enough extreme point to obtain envelopes from the

residual signal. The residual signal is calculated as follows:

$$\text{res}(m, n) = \text{input}(m, n) - \text{IMF}_i(m, n) \quad (5)$$

Figure 2 shows IMF signals obtained after EMD is applied to a seismic signal.

### 2.3 Mean Teager–Kaiser Energy Operator

TKEO is a powerful nonlinear operator which has been used successfully in different applications [37, 38]. TKEO is very interesting because of its simple definition, it is easy to implement and appears to be very strong in certain cases

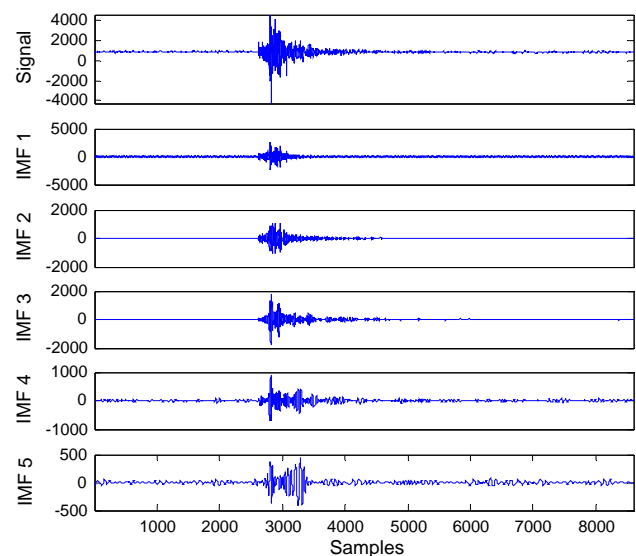


**Fig. 2** The EMD analysis of a seismic signal

of signal processing. TKEO has a good compatibility against high time resolution and sudden changes in signals. An important feature of the TKEO is that it is almost instantaneous, because only three samples are required each moment for energy calculation. Moreover, this simple operator allows the capturing of energy fluctuations as well as being efficient in practice. For a given band-limited discrete signal  $y[n]$ , the discrete form of the TKEO introduced by Kaiser [39] is given by:

$$\psi[y(n)] = y[n-1]^2 - y[n]y[n-2] \quad (6)$$

where  $\psi[y(n)]$  is called the TKEO coefficient of  $y[n]$ . In this study, the Mean TKEO which has been developed by Gardner is used. Logarithmic scaling is used in this algorithm for attribute normalization. The equation of Mean TKEO is given in Eq. (7).

$$\psi[y(n)] = \log\left(\frac{1}{N} \sum_{m=m-N+3}^n y[n-1]^2 - y[n]y[n-2]\right) \quad (7)$$

where  $y[n]$  is an seismic time series, and  $N$  is the window length.

#### 2.4 Proposed method: combining empirical mode decomposition and mean Teager–Kaiser energy operator

In this study, a new algorithm has been developed for hybrid use of EMD and Mean TKEO algorithms in seismic signal analysis. The algorithm has been implemented to detect P and S wave arrival times in seismic signals. In the study,

experiments have been carried out with numerous algorithms for the detection of the method that gives the best result. For example, wavelet transformation, Fourier transform, and EMD algorithms were used at the stage of obtaining features from the signal. Different energy operators were used for the changes in the sub-band signals. In the experiments, it is seen that effective results are obtained in the case of EMD and TKEO being used together. First of all, the signal is divided into windows consisting of 64 samples. The number of samples in the windows has been kept low for a more accurate determination. IMF signals obtained in 5 levels were examined with the implementation of EMD into each window. After that, Mean TKEO values of each window were calculated. From the observations, it is seen that P and S waves are clearly seen especially at the maximum TKEO values of IMF3 signals. The proposed method has been developed with this principle. The block diagram of the proposed method is given in Fig. 3. Accordingly, the processing steps are listed below.

- **Windowing and data preprocessing:** In the first phase, the signal is divided into windows of 64 samples. After the windowing process, the signal is cleared of noises at the preprocessing stage. By employing a 10-point noncausal moving average filter, the preprocessing stage was used to smooth the seismic signal. A 10th order IIR Butterworth band-pass filter, at the frequency ranges of 0.1–40 Hz, was applied to the seismic signals to remove the noise and artifacts from seismic signals.
- **Window Detection:** After the preprocessing step, EMD algorithm has been applied to each window and 5 levels

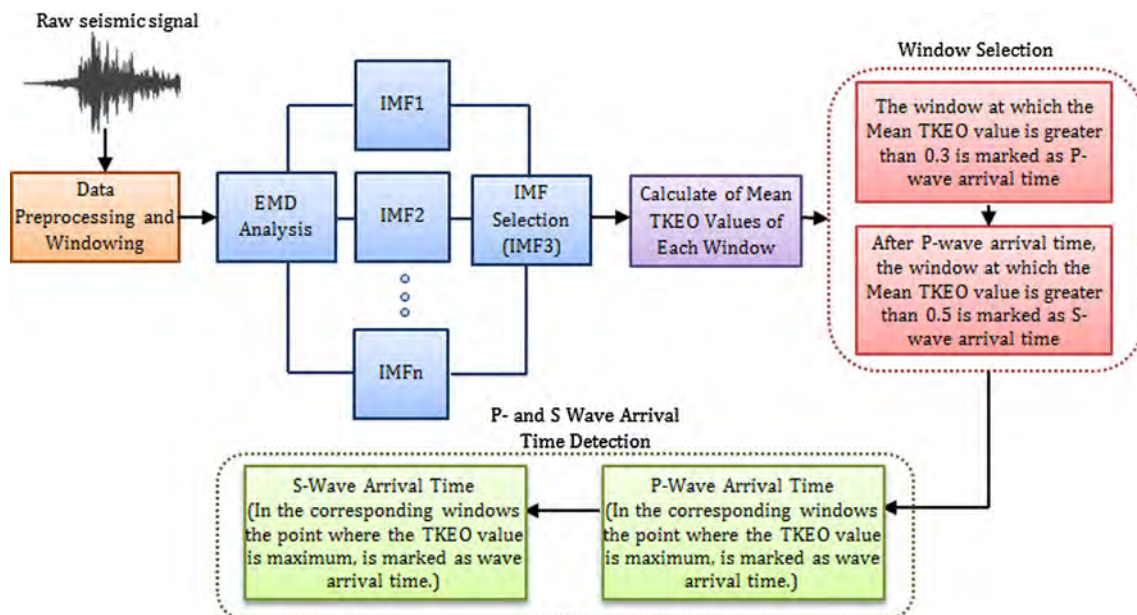


**Fig. 3** The block diagram of the proposed method

of IMF values have been obtained. The process was carried out on IMF3 signals. Mean TKEO values of each window were calculated. As a result of numerous trials, a threshold level has been set for P and S wave arrival times. Accordingly, the window in which the Mean TKEO value is greater than 0.3 (for the first time) is marked as the P wave arrival time. After the P wave arrival time, the window in which the Mean TKEO value is greater than 0.5 (for the first time) is marked as the S wave arrival time.

- P and S arrival time detection: It is unclear at which point of the window these two wave arrival times occur. A new method has been developed for this. In the corresponding windows the point where the TKEO value is maximum, is marked as wave arrival time. Observations performed in the experiments have led to this assumption. According to the suggested algorithm, if these components are considered comprehensively, the P and S wave arrival times can be computed as;

$$T_{P/S} = (n - 1)w + r \tag{8}$$

where  $T_{P/S}$  is P or S wave arrival time,  $n$  is the number of the detected window,  $w$  is window width, and  $r$  is the number of data in the maximum TEOG.

### 3 Application and experimental results

Two examples representing all of the results most effectively are discussed below.

#### 3.1 Case study 1

The Bala–Ankara/Turkey earthquake happened at 30.07.2005/23:30:38. Information about the earthquake is given in Table 1.

The east–west component of this seismogram is presented in Fig. 4 for ANTO station.

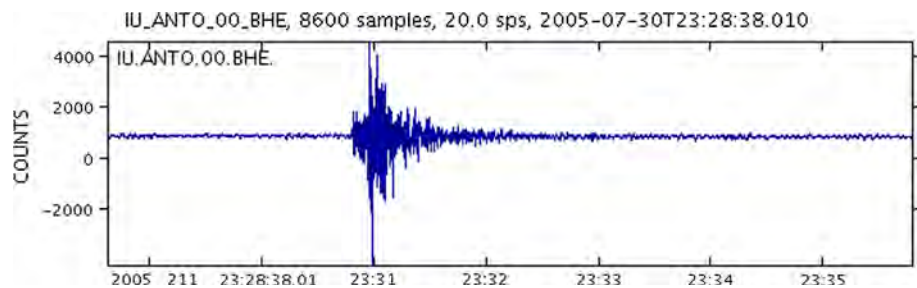
The signal which is given in Fig. 4 consists of a total of 8400 samples. This signal is divided into windows of 64 samples. After the preprocessing stage, EMD algorithm has been applied to the signal and IMF values have been obtained in 5 levels. Mean TKEO values of obtained IMF3 signals were calculated. The obtained chart is shown in Fig. 5.

In Fig. 5, a sudden increase of energy is observed in the windows that have been detected as P and S wave arrival times. The 37th window where the Mean TKEO value is greater than 0.3 for the first time is marked as the P wave arrival time window. After the P wave arrival time, the

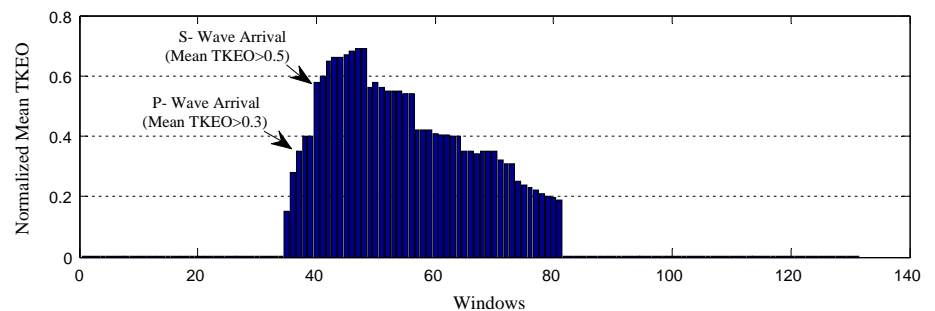
**Table 1** Information about the Bala–Ankara/Turkey earthquake

Network	Station code	Magnitude	Latitude	Longitude	Seismometer
IU	ANTO	3.5	39.87°	32.79°	Geotech KS 36000-I Borehole Seismometer

**Fig. 4** 30 July 2005, Bala/Ankara earthquake, east–west component, ANTO station, Ankara, latitude = 39.87, longitude = 32.79, magnitude = 3.5



**Fig. 5** Determination of windows containing P and S wave arrival times



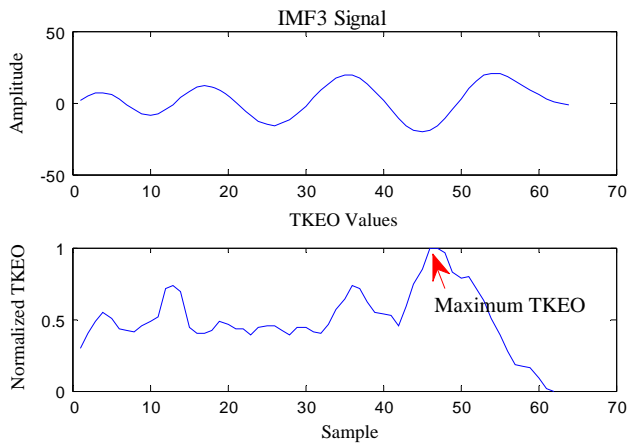


**Fig. 6** Finding of P wave arrival time point for experiment 1

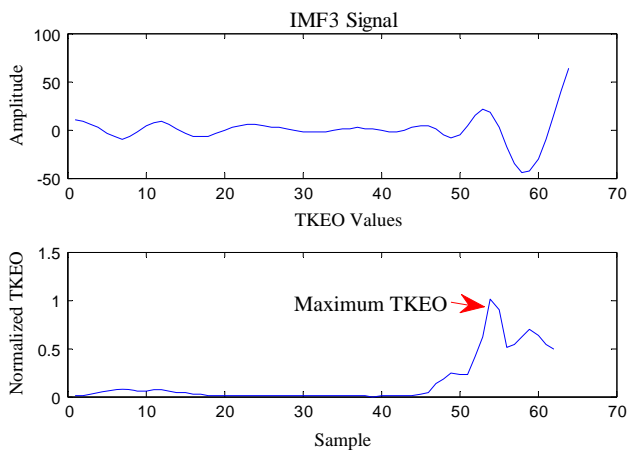


**Fig. 7** Finding of S wave arrival time point for experiment 1

40th window where Mean the TKEO value is greater than 0.5 for the first time is marked as the S wave arrival time window. It is unclear at exactly which point of the window these two waves occur. Equation (4) is used for the detection of this point. Maximum TKEO values obtained in the corresponding windows are shown in Figs. 6 and 7 for P and S waves. Accordingly, the arrival time of the P wave is the 47th sample of the 37th window. The arrival time of the S wave is the 54th point of the 40th window. According to Eq. 4, the P wave arrival time is obtained as  $(37 - 1) \times 64 + 47 = 2351$ th data. This point corresponds to the time 23:30:48.6. According to Eq. 4, the S wave arrival time is obtained as  $(40 - 1) \times 64 + 54 = 2550$ th data. This point corresponds to the time of 23:30:56.5.

Representation of detected P and S wave arrival time points on the signal is presented in Fig. 8. Related area enlarged from the original signal for a better look of the points.

The original representation of P and S wave arrival times that are manually detected by analysts for the same signal is presented in Fig. 9.

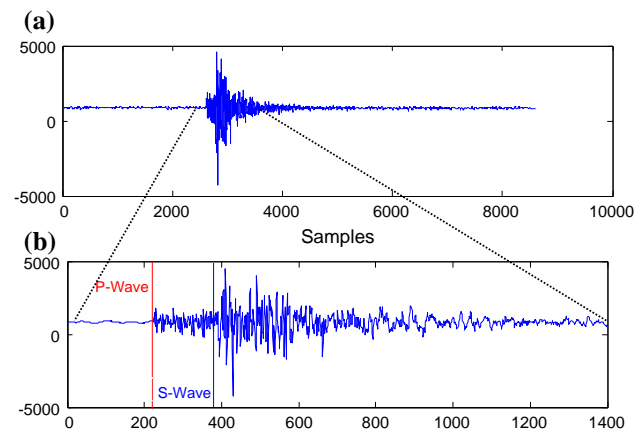


**Fig. 8** **a** Time series of the seismic signal. **b** P wave and S wave arrival of the original time series for that signal is zoomed

As shown in Figs. 8 and 9, automatically detected P and S wave arrival times are almost identical to the result achieved by the experts. The numerical difference between the two results is presented in Table 2.

### 3.2 Case study 2

The Orta–Cankiri/Turkey earthquake occurred at 06.06.2000/02:41:50. Information about the earthquake is given in Table 3.

The east–west component of this seismogram is displayed in Fig. 10 for KIEV station.

In the example that has been given, the signal consists of a total of 8400 samples. Firstly, this signal is divided into windows of 64 samples. The preprocessing stage has been carried out in each window to eliminate the noises in the signal. After that, the EMD algorithm was applied to the signal and IMF signals were obtained in 5 levels. Because IMF3 signals are taken into account in proposed method, the process in the next step is carried out on only based on IMF3 signals. Mean TKEO values of these signals were calculated in the next stage. The obtained graph is shown in Fig. 11.

These are a sudden energy increase in the windows determined as P and S wave arrival times in Fig. 11. The 37th window where the Mean TKEO value is greater than 0.3 for the first time is marked as the P wave arrival time window. After the P wave arrival time, the 74th window where the Mean TKEO value is greater than 0.5 for the first time is determined as the S wave arrival time window. Equation (4) is used in order to determine at which point of the window these two waves occur. Maximum TKEO values obtained in the corresponding windows are shown in Figs. 12 and 13 for P and S waves, respectively. Accordingly, arrival time of the P wave is the 41st sample of the 37th window. Arrival time of the S wave is the 56th point of the 74th window. According to Eq. (4), the P wave

**Fig. 9** Marking of P and S wave arrival times detected by the analyst in the original time series

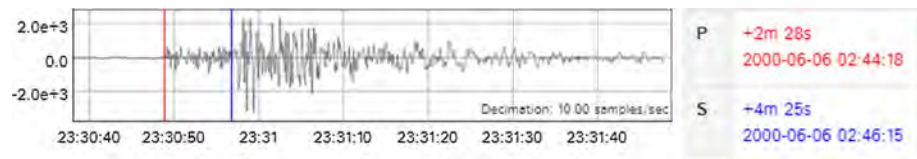


**Table 2** The numerical difference between the proposed method and manual analysis

Bala/Ankara Earthquake	P wave arrival ( $T_P$ ) (s)	S wave arrival ( $T_S$ ) (s)	$T_S - T_P$ (s)
Analyst	23:30:48	23:30:56	8
Proposed Method	23:30:48.5	23:30:56.4	7.9

**Table 3** Information about the Orta–Cankiri/Turkey earthquake

Network	Station code	Magnitude	Latitude	Longitude	Seismometer
IU	KIEV	6	50.70°	29.22°	Streckeisen STS-1H/VBB Seismometer

**Fig. 10** 06 June 2005, Orta–Cankiri earthquake, east–west component, KIEV station, Ukraine, latitude = 50.70, longitude = 29.22, magnitude = 6

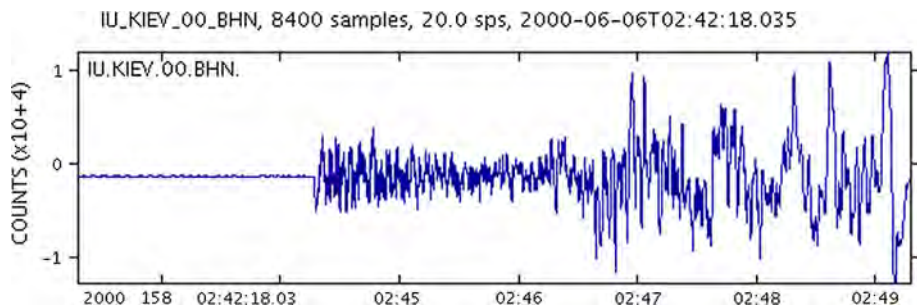
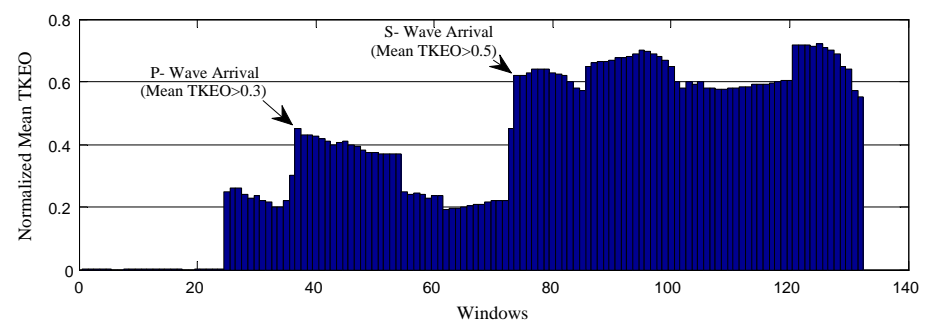


**Fig. 11** Determination of windows containing P and S wave arrival times



arrival time is obtained as  $(37 - 1) \times 64 + 41 = 2345$ th data. This point corresponds the time 02:44:18.5. According to Eq. (4), the S wave arrival time is obtained as  $(74 - 1) \times 64 + 56 = 4728$ th data. This point corresponds the time of 02:46:15.2.

Representation of the detected P and S wave arrival time points on the signal is presented in Fig. 14. A related area enlarged from the original signal for a better view of the points.

The representations of P and S wave arrival times that were manually detected by analysts for the same signal are presented in Fig. 15.

As shown in Figs. 14 and 15, automatically detected P and S wave arrival times are almost identical to the result

achieved by the experts. The numerical differences between the two results are presented in Table 4.

### 3.3 Results and comparison with other algorithms

The results of the study have been applied to 1000 different earthquakes and are presented in Table 5. Error detection between the recommended method and the manual analysis made by the analyst has been carried out based on time. Accordingly, the comparison was made on 4 time intervals. These time periods are as follows, respectively: 0–0.12, 0.13–0.22, 0.23–0.7, and >0.7 s.

Correct picks in Table 5 are the success rate (error amount is less than 0.7 s) in the comparison. Every second

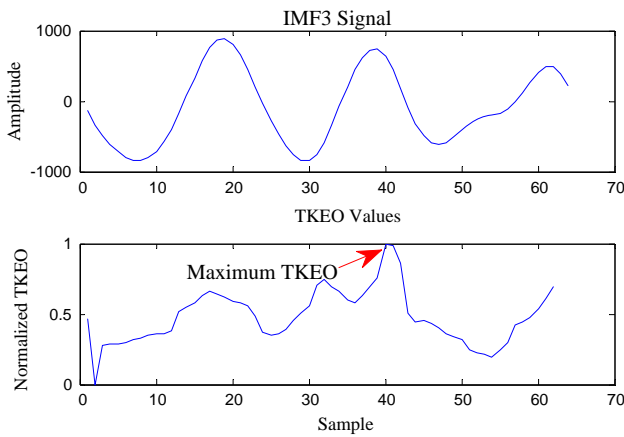


**Fig. 12** Finding of P wave arrival time point for experiment 2

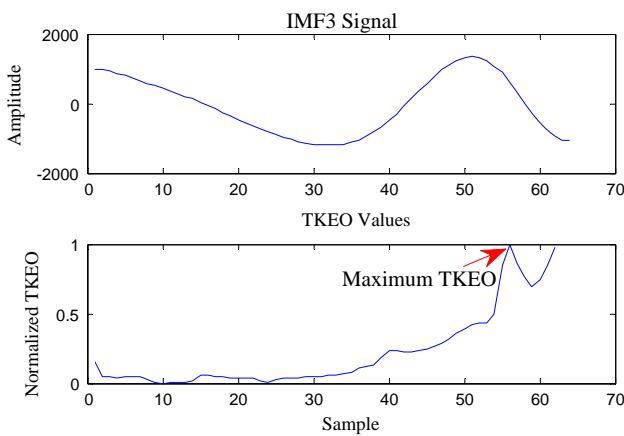


**Fig. 13** Finding of S wave arrival time point for experiment 2

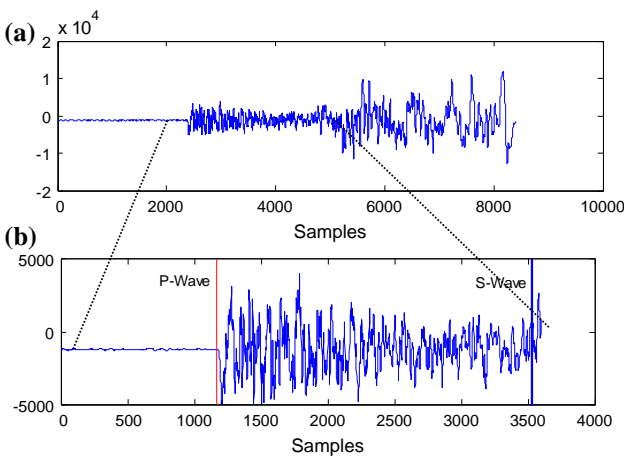


**Fig. 14** **a** Time series of the seismic signal. **b** P wave and S wave arrival of the original time series for that signal is zoomed

interval includes a percentage of this correct pick. For example, correct picks is 91 % for P wave arrival time detection. This indicates that 910 event out of the 1000

have been detected with an error rate of less than 0.7 s. Within these 910 events, 77.4 % (705 events) were between 0 and 0.12 s. 15 % (136 events) were between 0.13 and 0.22 s. 7.6 % (69 events) were between 0.23 and 0.7 s. The success of S wave arrival time detection is low compared to P wave arrival time detection.

For better evaluation of the performance of the proposed system, we compared it with the most commonly used and well-known automatic phase-picking algorithms. These algorithms include Allen’s algorithm [20], PAI-S and PAI-K [31]. Because these algorithms are mostly developed for identifying the P wave arrival time, the comparison has been made according to this arrival time. To facilitate the comparison, this chapter provides a brief summary of each algorithm.

Allen [20] has introduced the concept of characteristic function (CF) defined as the sum of the square of the seismic signal and the weighted square of its first derivative. Allen’s algorithm does not directly use its CF to determine phase arrival times, instead it uses STA/LTA rates of CF. STA/LTA algorithm (short-time average/long-time average) is a triggering method used in seismology for the analysis of the seismic data. Arrival time is determined when STA/LTA ratio exceeds the threshold which is empirically determined. This algorithm is still used today in practice. A detailed description of Allen’s algorithm is also available in [20].

PAI-S and PAI-K algorithms are based on higher order statistics, and these two algorithms take into account especially the values of skewness and kurtosis [31]. Skewness measures the symmetry of the distribution while kurtosis measures its tail-heaviness. The basic idea of the method is that the background noise almost follows the Gaussian distribution, and therefore, its skewness and kurtosis tend to zero. In contrast, P wave arrival time removes the Gaussian distribution of the time series and converts the distribution to an asymmetric heavy tailed one. As a result, the related skewness and kurtosis drastically increase. A PAI-S and PAI-K sliding time window is used to estimate skewness and kurtosis of the seismic path/trace. The maximum value of skewness and kurtosis is reached only when the time window contains a sufficient portion of the seismic signal. As described in [31], P arrival is picked at maximum slope. However, according to experiment, skewness and kurtosis sometimes can give local and global maximum point (which is not necessary to obtain) on P phase. To avoid incorrect choice, a threshold  $\delta$  (see Table 6) has been used for accurate detection of the peak point and then to use the position of that slope.

Comparisons have been carried out on the same data set. Each algorithm has a set of its parameters. Some of these parameters were set via optimization during the experiment [40]. To make the results more comparable, the parameters and all the values used for this study are given Table 6.



**Fig. 15** Original representation of P wave and S wave arrival times detected by analyst

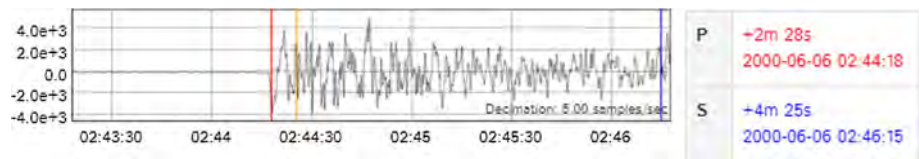


**Table 4** The numerical difference between proposed method and manual analysis

Orta/Cankiri earthquake	P wave arrival ( $T_p$ ) (s)	P wave arrival ( $T_p$ ) (s)	$T_s - T_p$ (s)
Analyst	02:44:18	02:46:15	117
Proposed method	02:44:18.5	02:46:15.2	116.7

**Table 5** Success rate of P wave arrival time detection

	Correct picks (%)	0–0.12 s (%)	0.13–0.22 s (%)	0.23–0.7 s (%)
P wave arrival time detection	91	77.4	15	7.6
S wave arrival time detection	86	75.5	13.6	10.9

**Table 6** Parameters of the algorithms used in this study

Algorithm	Parameters	Description	Values
Allen’s picker	$\theta$	Sliding pitch	$\theta = 0.015$ s
	$\alpha$	STA length	$\alpha = 0.2$ s
	$\beta$	LTA length	$\beta = 10$ s
	$C_3$	STA coefficient	$C_3 = 0.25$
	$C_4$	LTA coefficient	$C_4 = 0.004$
	$T_{min}$	Minimum signal length required	$T_{min} = 1.5$ s
PAI-K	$\theta$	Sliding pitch	$\theta = 0.015$ s
	$T$	Window length	$T = 3$ s
	$\delta$	Threshold	$1 < \delta < 7$
PAI-S	$\theta$	Sliding pitch	$\theta = 0.015$ s
	$T$	Window length	$T = 3$ s
	$\delta$	Threshold	$0.5 < \delta < 2.5$

**Table 7** Comparisons of the proposed algorithm with other very well-known methods

Algorithm	Correct picks (%)	0–0.12 s (%)	0.13–0.22 s (%)	0.23–0.7 s (%)
Allen (%)	81	68.5	21.2	10.3
PAI-K (%)	85	76.2	19.5	4.3
PAI-S (%)	83	75.8	20.4	3.8
Proposed method (%)	91	77.4	20.2	2.4

The results achieved by the analyst and the results obtained with the specified algorithms are compared in Table 7. As can be seen from Table 7, the proposed method has given very good results compared to others. 91 % of the incoming P waves were predicted accurately. 77.4 % of the correctly estimated P wave arrival times are detected with an error of less than 0.11 s. The lowest success rate was obtained with the Allen’s algorithm. Even though Allen’s algorithm is set to detect small

variations, it failed to choose the exact location of P wave arrival. This is because the characteristic function does not change enough at the beginning of the P wave. PAI-K/S algorithms gave better results compared to Allen’s algorithm. However, these algorithms showed a lower performance compared to proposed algorithm. These outcomes indicate that the accuracy of the proposed algorithm is superior to other algorithms used in seismic networks.

### 3.4 Limitations and future research directions

There are some limitations of this system. The success of the proposed method has been evaluated. The usability of the system should be increased in order to be used in real life. There is a need for a visual interface in order for experts to be able to use the software. For future studies, the aim is to develop a visual interface for the proposed model.

Also, the processing time of the program is advised to be low in order to increase the applicability. When experimental results are examined, it is seen that computation time of the proposed method is low. For example, for 420 s of data that consists of 8400 samples, P and S wave arrival time points are determined within about 0.05 s. Because the subject that has been worked on is a vital subject and it needs quick determination such as an earthquake, further reduction of the computation time is important. Therefore, the aim in further studies is acceleration of processes with CUDA programming which is a new GPU technology.

The proposed method was applied to a data set with a high noise ratio. But, its success on less noisy or moderately noisy data has not been evaluated. The success of the proposed method on different noise levels will be evaluated in further studies.

## 4 Conclusions

The purpose of this study was to develop an effective and new method for detecting P and S wave arrival times (with high accuracy values) which is an important problem in seismic signal analysis and used in earthquake prediction. The main novelty with regard to this study relates to the use of a hybrid method which integrates an effective decomposition method (EMD) and a strong energy operator (TKEO). The results obtained are promising. This system will help analysts in this field. The prominent parts of the study are as listed below:

Both P wave and S wave arrival time detection are possible with the proposed method. Only P arrival time detection has been carried out in many studies in the literature. There are small numbers of studies in S wave arrival time detection [41–45]. One of the main reasons is that S seismic waves move at a lower rate than P seismic waves and the noise ratio is higher than the S seismic waves. Moreover, the first S wave arrival can be hidden in P seismic waves [45]. The proposed system successfully determines the arrival time of these two waves, and it will make a significant contribution to the literature.

An algorithm based on complex mathematical calculations or based on training such as neural networks was not used in the developed method. Because the method is

based on simple mathematical functions, it allows fast operation of the system. The rapid detection of these two waves is important in an area of vital importance such as an earthquake.

The proposed hybrid systems gave better results compared to other methods in the literature. It is predicted that this proposed hybrid method will be a good source for many studies in seismic signal analysis.

### Compliance with ethical standards

**Conflicts of interest** The authors declare that they have no conflict of interests.

## References

1. Anant KS, Dowla FU (1997) Wavelet transform methods for phase identification in three-component seismograms. *Bull Seismol Soc Am* 87:1598–1612
2. Colak OH, Destici TC, Arman H, Cerezci O (2009) Detection of P-and S-waves arrival times using the discrete wavelet transform in real seismograms. *Arab J Sci Eng* 34:79–89
3. Erturk A, Gullu MK, Erturk S (2013) Hyperspectral image classification using empirical mode decomposition with spectral gradient enhancement. *IEEE Trans Geosci Remote Sens* 51:2787–2798
4. Ross ZE, Ben-Zion Y (2014) Automatic picking of direct P, S seismic phases and fault zone head waves. *Geophys J Int* 199:368–381
5. Ross ZE, Ben-Zion Y (2014) An earthquake detection algorithm with pseudo-probabilities of multiple indicators. *Geophys J Int* 197:458–463
6. Borchardt RD (1992) Anatomy of Seismograms. *Earthq Spectra* 8:495–496
7. Gelchinsky B, Shtivelman V (1983) Automatic picking of first arrivals and parameterization of traveltimes curves. *Geophys Prospect* 31:915–928
8. McCormack MD, Zaucha DE, Dushek DW (1993) First-break refraction event picking and seismic data trace editing using neural networks. *Geophysics* 58:67–78
9. Boschetti F, Dentith MD, List RD (1996) A fractal-based algorithm for detecting first arrivals on seismic traces. *Geophysics* 61:1095–1102
10. Tong C, Kennett BLN (1996) Automatic seismic event recognition and later phase identification for broadband seismograms. *Bull Seismol Soc Am* 86:1896–1909
11. Wagner GS, Owens TJ (1996) Signal detection using multi-channel seismic data. *Bull Seismol Soc Am* 86:221–231
12. Withers M, Aster R, Young C, Beiriger J, Harris M, Moore S, Trujillo J (1998) A comparison of select trigger algorithms for automated global seismic phase and event detection. *Bull Seismol Soc Am* 88:95–106
13. Hidani A, Yamanaka H (2003) Automatic picking of seismic arrivals in strong motion data using an artificial neural network. *Environmental Science and Technology*, Tokyo Institute of Technology
14. Zhang H, Thurber C, Rowe C (2003) Automatic P-wave arrival detection and picking with multiscale wavelet analysis for single-component recordings. *Bull Seismol Soc Am* 93:1904–1912
15. Takunami T, Kitagawa G (2003) Methods and applications of signal processing in seismic network operations. In: Bhattacharji S, Friedman GM, Neugebauer HJ, Seilacher A (eds) *Lecture Notes in Earth Sciences*, vol 98. Springer, Berlin, p 2003

16. Hafez AG, Khan MTA, Kohda T (2010) Clear P-wave arrival of weak events and automatic onset determination using wavelet filter banks. *Digit Signal Process* 20:715–723
17. Liu X (2013) Time-arrival location of seismic P-wave based on wavelet transform modulus maxima. *J Multimed* 8:32–39
18. Hafez AG, Rabie M, Kohda T (2013) Seismic noise study for accurate P-wave arrival detection via MODWT. *Comput Geosci* 54:148–159
19. Wong J, Han L, Bancroft JC, Stewart RR (2009) Automatic time-picking of first arrivals on noisy microseismic data. *STA* 2:1
20. Allen RV (1978) Automatic earthquake recognition and timing from single traces. *Bull Seismol Soc Am* 68:1521–1532
21. Magotra N, Ahmed N, Chael E (1987) Seismic event detection and source location using single-station (three-component) data. *Bull Seismol Soc Am* 77:958–971
22. Magotra N, Ahmed N, Chael E (1989) Single-station seismic event detection and location. *IEEE Trans Geosci Remote Sens* 27:15–23
23. Wang J, Teng T-L (1995) Artificial neural network-based seismic detector. *Bull Seismol Soc Am* 85:308–319
24. Zhao Y, Takano K (1999) An artificial neural network approach for broadband seismic phase picking. *Bull Seismol Soc Am* 89:670–680
25. Gentili S, Michellini A (2006) Automatic picking of P and S phases using a neural tree. *J Seismol* 10:39–63
26. Ahmed A, Sharma ML, Sharma A (2014) Wavelet based automatic phase picking algorithm for 3-component broadband seismological data. *J Seismol Earthq Eng* 9:15–24
27. Hafez AG, Khan TA, Kohda T (2009) Earthquake onset detection using spectro-ratio on multi-threshold time–frequency sub-band. *Digit Signal Process* 19:118–126
28. Xiantai G, Zhimin L, Na Q, Weidong J (2011) Adaptive picking of microseismic event arrival using a power spectrum envelope. *Comput Geosci* 37:158–164
29. Sleeman R, van Eck T (1999) Robust automatic P-phase picking: an on-line implementation in the analysis of broadband seismogram recordings. *Phys Earth Planet Inter* 113:265–275
30. Panagiotakis C, Kokinou E, Vallianatos F (2008) Automatic P-phase picking based on local-maxima distribution. *IEEE Trans Geosci Remote Sens* 46:2280–2287
31. Saragiotis CD, Hadjileontiadis LJ, Panas SM (2002) PAI–S/K: a robust automatic seismic P phase arrival identification scheme. *IEEE Trans Geosci Remote Sens* 40:1395–1404
32. Küperkoch L, Meier T, Lee J, Friederich W, Working Group, E (2010) Automated determination of P-phase arrival times at regional and local distances using higher order statistics. *Geophys J Int* 181:1159–1170
33. Taylor KM, Procopio MJ, Young CJ, Meyer FG (2011) Estimation of arrival times from seismic waves: a manifold-based approach. *Geophys J Int* 185:435–452
34. Incorporated Research Institutions For Seismology (IRIS) <http://ds.iris.edu/wilber3/>. Accessed 2 November 2014
35. An X, Yang J (2015) Denoising of hydropower unit vibration signal based on variational mode decomposition and approximate entropy. *Trans Inst Meas. Control.* 0142331215592064
36. Wang Z, Lu C, Wang Z, Liu H, Fan H (2013) Fault diagnosis and health assessment for bearings using the Mahalanobis–Taguchi system based on EMD-SVD. *Trans Inst Meas Control.* 0142331212472929
37. Jabloun F, Cetin AE, Erzin E (1999) Teager energy based feature parameters for speech recognition in car noise. *IEEE Signal Process Lett* 6:259–261
38. Bahoura M, Rouat J (2001) Wavelet speech enhancement based on the Teager energy operator. *IEEE Signal Process Lett* 8:10–12
39. Kaiser JF (1990) On a simple algorithm to calculate the ‘energy’ of a signal. In: 1990 international conference on acoustics, speech, and signal processing. ICASSP-90. vol 1, pp 381–384
40. Laasri EHA, Akhouayri E-S, Agliz D, Atmani A (2014) Automatic detection and picking of P-wave arrival in locally stationary noise using cross-correlation. *Digit Signal Process* 26:87–100
41. Cichowicz A (1993) An automatic S-phase picker. *Bull Seismol Soc Am* 83:180–189
42. Wang J, Teng T (1997) Identification and picking of S phase using an artificial neural network. *Bull Seismol Soc Am* 87:1140–1149
43. Tasic I, Grabec I (2000) Characterization of seismic waves arrival with simulated neural networks;. I. Ljubljana, Tasic
44. Saragiotis CD, Hadjileontiadis LJ, Savvaadis AS, Papazachos CB, Panas SM (2000) Automatic S-phase arrival determination of seismic signals using nonlinear filtering and higher-order statistics. In *Geoscience and Remote Sensing Symposium, 2000. Proceedings. IGARSS 2000. IEEE 2000 International.* vol 1, pp 292–294
45. Tasic I, Runovc F (2009) Automatic S-phase arrival identification for local earthquakes. *Acta Geotech Slov* 6:46–55
46. Aboamer MM, Azar AT, Wahba K, Mohamed ASA (2014) Linear model-based estimation of blood pressure and cardiac output for Normal and Paranoid cases. *Neural Comput Appl* 25(6):1223–1240. doi:10.1007/s00521-014-1566-4
47. Aboamer MM, Azar AT, Mohamed ASA, Bär KJ, Berger BS, Wahba K (2014) Nonlinear features of heart rate variability in paranoid schizophrenic. *Neural Comput Appl* 25(7–8):1535–1555. doi:10.1007/s00521-014-1621-1